Development Of Frequency And Time Domain Solvers For Integrated Optics

A Project Report

submitted by

MANDAR BELAMBE

in partial fulfilment of the requirements
for the award of the degree of

BACHELOR OF TECHNOLOGY

DEPARTMENT OF ELECTRICAL ENGINEERING

INDIAN INSTITUTE OF TECHNOLOGY MADRAS.

MAY 2014

THESIS CERTIFICATE

This is to certify that the thesis titled **Development of Frequencyand Time Domain Solvers for Integrated Optics**, submitted by**MANDAR BELAMBE**,to the Indian Institute of Technology, Madras, for the award of the degree of **Master Of Technology**, is a bonafide record of the research work done by him under our supervision. The contents of this thesis, in full or in parts, have not been submitted to any other Institute or University for the award of any degree or diploma.

Prof. Dr. Bijoy K. Das, Associate Professor, Department of Electrical Engineering, IIT-Madras, 600036

Place: Chennai

Date: 19th January 2009

ACKNOWLEDGEMENTS

I thank Prof. Bijoy K. Das for giving me this project to work on. I also thank Varun Singh, Shantanu Pal, Vivek PS for helping me work on different types of structures. I thank the other members of IOLAB, Electrical Department, IIT Madras, for their help during the project.

TABLE OF CONTENTS

LIST OF TABLES

LIST OF FIGURES

CHAPTER 1

Introduction

1.1 Silicon Photonics

In the last decade Silicon Photonics has emerged as an important area of research in the field of communication technology. As the device size becomes smaller, the gate delays, power consumption and other factors start causing problems for electronic systems. On the other hand optical interconnects have lower delays and have low power losses. As silicon is transparent to the communication wavelength($\lambda = 1.55 \times 10^{-6}$) , and the electronic devices are all based on silicon based technology, it is possible to create hybrid optical and electronic circuits on a single chip. While the optical device sizes are very big compared to electronic devices, due to high index contrast of silicon (n$\approx$3.477) it is possible to have submicron size optical devices in silicon. As the size of the optical device reduces, the optical field intensity confined within the optical device increases thus making the phenomena of non-linear effects more prominent during the propagation of light. Recently, different types of all optical switches in silicon have also been fabricated and verified, thus extending the silicon photonics research into the possibility of having all-optical logic circuits, thus eliminating the optical to electronic conversion delays. As the presence of electronic charges within an optical device affect its performance, it is also possible to have active optical devices in silicon. Due to the bulkiness of optical structures with respect to electronic structures, and given their advantages over the electronic structures, hybrid integrated optoelectronic devices on a single substrate is an important field of research.

1.2 Motivation

The modal calculation of optical waveguides is an important topic in the field of guided-wave optics. For optical waveguides, calculations of mode sizes, effective indices, group velocities etc are important for choosing optimal dimensions for the waveguides. There is a need for modeling techniques accurate for a wide range of structures. Analytic and semi-analytic methods are suitable for simple structures such as rib or ridge waveguides or optical fibers. But the advances in the photonics technologies have established the need for the development of numerical and approximate methods for the analysis of a wide range of waveguide structures that are not amenable to exact analytical studies. An efficient mode solver has to be easier to implement, easy to use, fast and should have smaller computational requirements. It should be able to provide all the fields in order to predict accurate propagation constants.

Among the various numerical methods, BPM (Beam Propagation Method), FEM (Finite Element Method) and FDMs (Finite Difference Methods) have been widely used. While FEM is better for non-regular structures and adaptive meshing, the formulations for FEM are quite complicated compared to Finite Difference Methods and may create solutions with spurious and non-physical modes. While BPM is more thorough, it requires more computational effort and has quite complex formulation as compared to FDMs. Also for High Index Contrast materials like Silicon, the paraxial approximation assumed in BPM may not be valid. For FDMs, once the governing equations and the boundary conditions are provided, it is straightforward to implement a finite difference scheme.

While large cross section waveguides (area of cross section $\approx 25\mu m^2$), have TE and TM modes where only one of the E_x, E_y fields is present, smaller cross-

section waveguides (e.g., photonic wire) have modes which have both E_x and E_y components of electric field, hence the need for Full vectorial solutions for modes. For the first case, the semi-vectorial mode solver has been developed since the coupling between the TE and TM modes is very small and can be neglected. For smaller dimensions, this is not the case and both E_x and E_y have to be found for correct prediction of effective index.

In any optical circuit, it is not possible to use only straight waveguides. For some applications bent waveguides are needed (e.g., ring resonators). To find out optimal dimensions (radius and cross-section dimensions) for these waveguides, again we need to use a mode solver. It has been found that a finite difference scheme similar to that used for straight waveguides can be developed and implemented in a very similar way.

While the thesis is centered mostly around silicon waveguides, it has also been found that the finite-difference scheme can be easily adjust to use with some anisotropic materials such as $LiNbO_3$ where the permittivity tensor has only diagonal elements and the diagonal elements are not all equal.

For simulation of waveguides, however, only the modes are not enough. We need to actually simulate the waveguides in time domain. This is possible using the mode solver using Mode Expansion methods. But it's not quite simple to include non-linearity in the simulations. However, using Auxiliary Differential Equation formulations it's possible to include the non-linearity in the FDTD (Finite-Difference Time-Domain) method itself.

As the photonics industry is moving towards silicon for integrated optics and optoelectronics, various optical effects are being measured for Silicon such as Kerr effect and Raman effect. The high optical intensity due to high index contrast between silicon (n$\approx$3.477) and SiO_2 (n$\approx$1.45), makes it possible to observe

the non-linear interactions in chip-scale devices. It is also established that the presence of free carriers affects the refractive index of the material and therefore the optical guiding properties. Thus it is important to simulate the non-linear characteristics of silicon waveguides.

Due to high computational and memory costs, the simulation of an entire structure in FDTD takes a long time (usually many hours). Therefore, it is also important to explore the possibility of implementing FDTD in other platforms than just a CPU. To this end, FDTD for large structures is usually implemented on clusters of CPUs. Since the advancement of GPUs (Graphics Processor Units) and their native computing languages, the simulations have been shown to speed up significantly.

1.3 Research Objectives

The Finite Difference Method is a very useful tool and it is quite easy to implement as well. The goal of the project is to implement the finite difference method for Maxwell's equations in both frequency domain and time domain as way to improve upon the existing methods for solutions for optical waveguides. Although the time domain method has been implemented for a while now, the non-linearity of silicon has not been implemented as a standard. The thesis looks towards the feasibility of time domain methods as a way to simulate non-linear structures.

1.4 Thesis Organization

The first chapter introduces a full-vectorial mode solver along with a semi-vectorial mode solver for a general waveguide cross-section. Here, the equations for the

mode solvers have been derived from Maxwell's Equations in frequency domain. Using a generalized relationship between the field at a point and its nearby points, we can construct an eigenvalue equation for the field(1). Both the mode solvers have been developed and implemented in MATLAB. The results have been compared with lumerical's mode solver and with analytical results as well wherever possible.

The second chapter deals with Finite Difference Time Domain (FDTD) method for simulation for silicon optical waveguides. Here, the linear polarization, non-linear polarization effects have been implented in the FDTD equations(3). The non-linear polarization effects included are Raman Effect, Kerr Effect, Two Photon Absorption, Free Carrier Absorption and Free Carrier Plasma Dispersion Effect. While Linear, Raman, Kerr effects have been implemented using Auxiliary Differential Equations (ADE) method, the plasma dispersion effect has been implemented using an iterative method. TPA and FCA have been implemented directly by inserting the related loss term in conductivity. The simulations were done in 2D using TM_Z mode. The update coefficients for TE_Z have been derived but not implemented. The simulation region has been terminated using Gedney's CPML(4). The method has been implemented for SOI photonic wire waveguide of dimensions $450nm \times 200nm$.

The Compound FDTD method has been implemented using MATLAB and a separate code has also been developed using OpenCL.

The final chapter presents conclusions and possible future works.

CHAPTER 2

Silicon Photonics:Full Vectorial Finite Difference Method

2.1 Introduction

Most common waveguide structure in Silicon photonics are the rib and the ridge structures. Because of rectangular meshing used in the FDM, this method is very suitable for the silicon waveguide structures. For calculating the modes of a waveguide, the cross-section of the waveguide is used. The mode size and shape as well as the refractive index of the waveguide are defined for a single wavelength, ie for a single frequency. Therefore, solving the Maxwell's equations in the frequency domain will give the solution for the modes.

The figure **??** shows a general rib waveguide structure used in the FDM formulation. In general, the cross section can have any arbitrary shape, but due to rectangular grid used, the structure solved for will actually have only rectangular edges.

2.2 Maxwell's Equations

We start with the Maxwell's Equations in frequency domain.

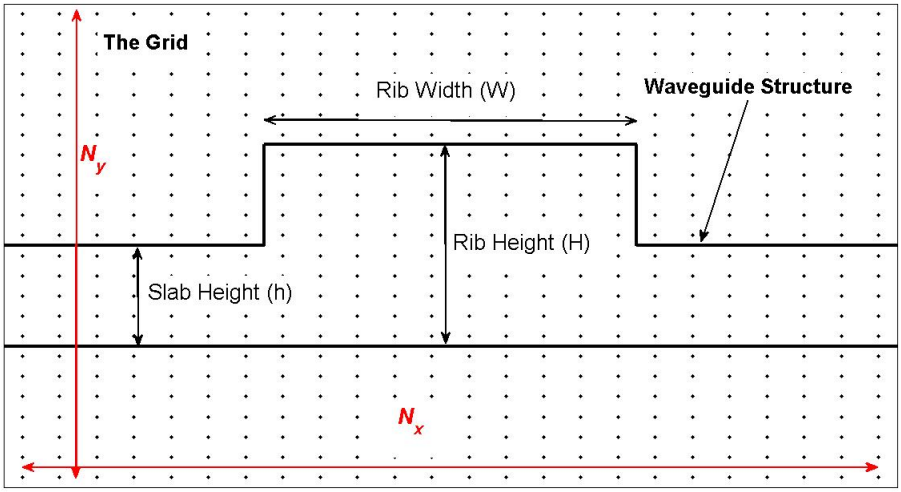

Figure 2.1: Grid and the waveguide structure used in the FDM

$$\nabla.\vec{D} = 0 \tag{2.1}$$

$$\nabla.\vec{H} = 0 \tag{2.2}$$

$$\nabla \times \vec{E} = -\jmath\mu_0\omega\vec{H} \tag{2.3}$$

$$\nabla \times \vec{H} = (\sigma + \jmath\omega\epsilon)\vec{E} \tag{2.4}$$

For calculation of effective index for a straight waveguide we consider certain assumptions,

For a lossless waveguide,

$$\sigma = 0 \tag{2.5}$$

for a straight waveguide,

$$\frac{\partial \epsilon}{\partial z} = 0 \tag{2.6}$$

for a guided mode,

$$\vec{E} \sim \vec{E}(x,y)e^{j(\omega t - \beta z)} \tag{2.7}$$

Using equations (2.5,2.6) with equation (2.1), we get

$$\begin{aligned}
\frac{\partial(\epsilon E_x)}{\partial x} + \frac{\partial(\epsilon E_y)}{\partial y} + \frac{\partial(\epsilon E_z)}{\partial z} &= 0 \\
\frac{\partial(\epsilon E_x)}{\partial x} + \frac{\partial(\epsilon E_y)}{\partial y} + \epsilon\frac{\partial(E_z)}{\partial z} + E_z\frac{\partial(\epsilon)}{\partial z} &= 0 \\
\frac{\partial(\epsilon E_x)}{\partial x} + \frac{\partial(\epsilon E_x)}{\partial x} &= \jmath\beta\epsilon E_z \\
E_z &= \frac{1}{\jmath\beta\epsilon}\left(\frac{\partial(\epsilon E_x)}{\partial x} + \frac{\partial(\epsilon E_y)}{\partial y}\right)
\end{aligned} \tag{2.8}$$

Therefore we have $E_z$in terms of $E_x$and E_y.

Expanding equation (2.8) into its scalar components gives,

$$-\jmath\omega\mu_0 H_x = \left(\frac{\partial E_z}{\partial y} - \frac{\partial E_y}{\partial z}\right) \tag{2.9}$$

$$-\jmath\omega\mu_0 H_y = \left(\frac{\partial E_x}{\partial z} - \frac{\partial E_z}{\partial x}\right) \tag{2.10}$$

$$-\jmath\omega\mu_0 H_z = \left(\frac{\partial E_y}{\partial x} - \frac{\partial E_x}{\partial y}\right) \tag{2.11}$$

Using Equations (2.9) and (2.10) with equation (2.8) gives values of H_x,$H_y$and H_z.

Thus, once we know the values of $E_x$and $E_y$profiles , we can calculate the remaining field values.

2.3 The Wave Equations

Taking curl of equation (2.3), and using equation (2.4), we get

$$\begin{aligned} \nabla \times (\nabla \times \vec{E}) &= -\jmath\omega\mu_0 \nabla \times \vec{H} \\ \nabla \times (\nabla \times \vec{E}) &= -\jmath\omega\mu_0 (\jmath\omega\epsilon\vec{E}) \\ \nabla(\nabla.\vec{E}) - \nabla^2\vec{E} &= \omega^2\mu_0\epsilon\vec{E} \end{aligned} \tag{2.12}$$

using equation (2.1) again to calculate $\nabla.\vec{E}$, we get

$$\begin{aligned} \nabla.(\epsilon\vec{E}) &= 0 \\ \epsilon\nabla.\vec{E} + \vec{E}.\nabla\epsilon &= 0 \\ \nabla.\vec{E} &= -\vec{E}.\frac{\nabla\epsilon}{\epsilon} \end{aligned} \tag{2.13}$$

Equation (2.12) combined with equation (2.13) gives,

$$\nabla^2\vec{E} + \nabla(\quad \vec{E}.\tfrac{\nabla\epsilon}{\epsilon}) + (\omega^2\mu\epsilon)\vec{E} = \quad 0 \tag{2.14}$$

Since E_z can be calculated once $E_x$and $E_y$are found, we can use this equation as the basis for calculating mode profiles for guided modes of a straight waveguide.

Expanding equation (2.14) into its components,using equation (2.7)

$$\frac{\partial^2}{\partial x^2}E_x + \frac{\partial^2}{\partial y^2}E_x + \frac{\partial}{\partial x}\left(\frac{E_x}{\epsilon}\frac{\partial\epsilon}{\partial x} + \frac{E_y}{\epsilon}\frac{\partial\epsilon}{\partial y}\right) + (\omega^2\mu\epsilon - \beta^2)E_x = 0 \tag{2.15}$$

$$\frac{\partial^2}{\partial x^2}E_y + \frac{\partial^2}{\partial y^2}E_y + \frac{\partial}{\partial y}\left(\frac{E_x}{\epsilon}\frac{\partial\epsilon}{\partial x} + \frac{E_y}{\epsilon}\frac{\partial\epsilon}{\partial y}\right) + (\omega^2\mu\epsilon - \beta^2)E_y = 0 \tag{2.16}$$

Equations (2.15) and (2.16) are discretized and converted to eigen equation form of type $\boldsymbol{A}\boldsymbol{x} = \lambda\boldsymbol{x}$.

2.3.1 Formulation For Full-vectorial Mode Solver

For full-vectorial mode solver, we do not ignore any of the terms in equations (2.15) and (2.16).

Before converting equations (2.15) and (2.16) to finite difference form, we rearrange the terms using the following identity.

$$\frac{\partial^2}{\partial x^2}\Psi + \frac{\Psi}{\Phi}\frac{\partial \Phi}{\partial x} = \frac{\partial}{\partial x}(\frac{1}{\Phi}\frac{\partial}{\partial x}(\Phi\Psi))$$

Equations (2.15) and (2.16) become,

$$\frac{\partial^2}{\partial y^2}E_x + \frac{\partial}{\partial x}\left(\frac{1}{\epsilon}\left(\frac{\partial}{\partial x}(\epsilon E_x) + \frac{\partial}{\partial y}(\epsilon E_y)\right)\right) - \frac{\partial^2}{\partial x \partial y}E_y + (\omega^2\mu\epsilon - \beta^2)E_x = 0 \tag{2.17}$$

$$\frac{\partial^2}{\partial x^2}E_y + \frac{\partial}{\partial y}\left(\frac{1}{\epsilon}\left(\frac{\partial}{\partial x}(\epsilon E_x) + \frac{\partial}{\partial y}(\epsilon E_y)\right)\right) - \frac{\partial^2}{\partial x \partial y}E_x + (\omega^2\mu\epsilon - \beta^2)E_y = 0 \tag{2.18}$$

Equations (2.17) and (2.18) are discretized using 9-point stencil to get equations of the following form,

$$\sum_i \sum_j \left(A_{xx}^{ij}E_x^{ij} + A_{xy}^{ij}E_y^{ij}\right) = \beta^2 E_x \tag{2.19}$$

$$\sum_i \sum_j \left(A_{yx}^{ij}E_x^{ij} + A_{yy}^{ij}E_y^{ij}\right) = \beta^2 E_y \tag{2.20}$$

In (2.19) and (2.20), $i = p-1, p, p+1$ and $j = q-1, q, q+1$ as shown in the

figure **??**.

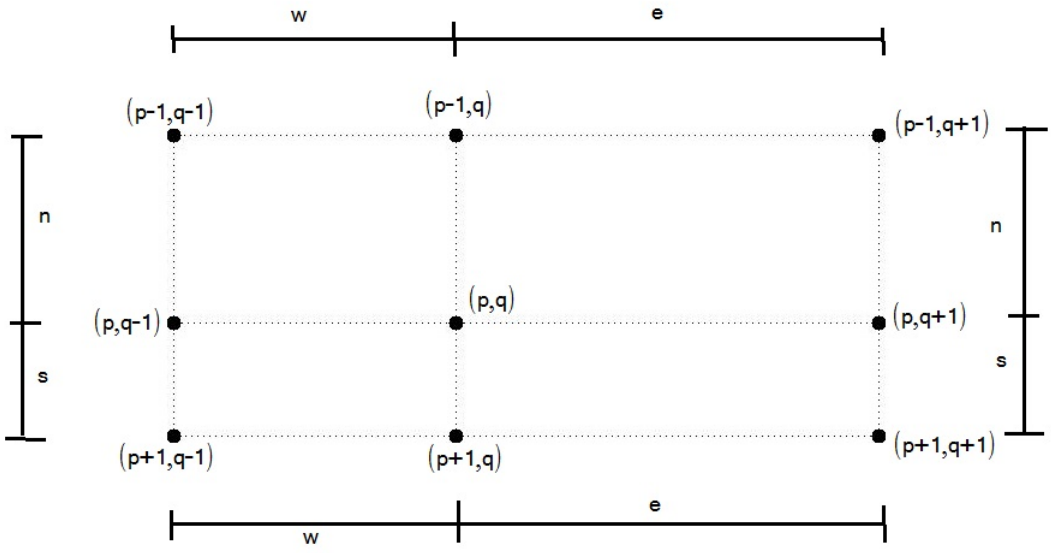

Figure 2.2: Grid used for Discretization of the wave equations.
The Fields E_x, E_y as well as the permittivity ϵ_r are defined at lattice points in the above grid.

Equations (2.19) and (2.20) together form an eigenvalue equation of the following form,

$$\boldsymbol{A\Phi} = \beta^2\boldsymbol{\Phi} \tag{2.21}$$

Where,

$$\boldsymbol{A} = \begin{bmatrix} \boldsymbol{A_{xx}} & \boldsymbol{A_{xy}} \\ \boldsymbol{A_{yx}} & \boldsymbol{A_{yy}} \end{bmatrix}$$

and

$$\mathbf{\Phi} = \begin{bmatrix} \boldsymbol{E_x} \\ \boldsymbol{E_y} \end{bmatrix}$$

Equation (2.21) is the final equation used to calculate full-vectorial mode profiles and effective index.

Effective indices of different modes can be found using the eigenvalues of this equation, while electric fields corresponding to these effective indices can be found from corresponding eigenvectors.

Here, length of field array used in equation (2.21) is $(2 \times N_x \times N_y)$. Therefore, size of the $\boldsymbol{A}$ matrix is $((2 \times N_x \times N_y) \times (2 \times N_x \times N_y))$, which is 4 times the size of $\boldsymbol{A}$ matrices used in semivectorial mode solver.

Since we are using 9 point stencil, maximum number of non-zero elements in any row of $\boldsymbol{A}$ is 9.

For 2-D confined waveguides, we need a 2 dimensional array of field. But, the field arrays used in equation (2.21) are column vectors. Therefore, we need to linearize the field arrays to use in equation (2.21). After calculating the mode profiles, we need to convert them back to 2-D. The linearization scheme used is shown in the figure **??**.

2.3.2 Formulation for Semi-vectorial mode solver

For large cross section high refractive index waveguides, the modes can be separated into TE and TM modes. In terms of the fields, this means that for TE modes $E_x$field will be dominant while for TM modes E_y field will be dominant. Thus, equations (2.15) and (2.16) can be decoupled to get separate equations for TE and

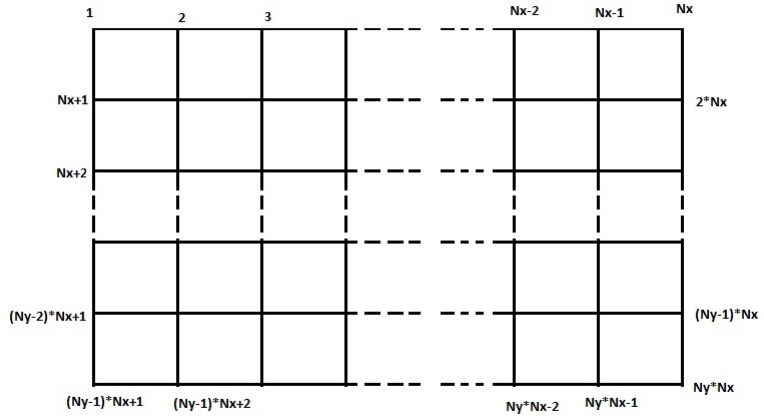

Figure 2.3: index linearization scheme

TM modes.

$$\frac{\partial^2}{\partial x^2}E_x + \frac{\partial^2}{\partial y^2}E_x + \frac{\partial}{\partial x}\left(\frac{E_x}{\epsilon}\frac{\partial \epsilon}{\partial x}\right) \quad +(\omega^2\mu\epsilon - \beta_{TE}^2)E_x = \quad 0 \qquad (2.22)$$

$$\frac{\partial^2}{\partial x^2}E_y + \frac{\partial^2}{\partial y^2}E_y + \frac{\partial}{\partial y}\left(\frac{E_y}{\epsilon}\frac{\partial \epsilon}{\partial y}\right) \quad +(\omega^2\mu\epsilon - \beta_{TM}^2)E_y = \quad 0 \qquad (2.23)$$

since the cross coupling terms are negligible.

$$\frac{\partial}{\partial x}\frac{E_y}{\epsilon}\frac{\partial \epsilon}{\partial y} \approx 0$$

$$\frac{\partial}{\partial y}\frac{E_x}{\epsilon}\frac{\partial \epsilon}{\partial x} \approx 0$$

Since here we need partial derivatives along only one dimension in any of terms in equations (2.22) and (2.23), we can use 5 point stencil here.

Equations (2.22) And (2.23) are discretized to give equations of the following form for TE and TM modes.

$$\boldsymbol{A_x E_x} = \beta_{TE}^2 \boldsymbol{E_x} \tag{2.24}$$

$$\boldsymbol{A_y E_y} = \beta_{TM}^2 \boldsymbol{E_y} \tag{2.25}$$

Equations (2.24) and (2.25) are eigen equations and therefore can be solved using eigenvalue solvers in linear algebra libraries. Effective indices of different modes can be found using the eigenvalues of these equations, while electric fields corresponding to these effective indices can be found from corresponding eigenvectors.

It should be noted that for a grid of size $(N_x \times N_y)$, the eigenvector length is $(N_x \times N_y)$. Therefore, the size of $\boldsymbol{A_x}$and $\boldsymbol{A_y}$ matrices is $((N_x \times N_y) \times (N_x \times N_y))$. Also, since we are using 5 point stencil, maximum number of non-zero elements in any row of $\boldsymbol{A_x}$and $\boldsymbol{A_y}$ is 5.

2.3.3 Full-Vectorial Mode Solver For Anisotropic Media

In this section, the full vectorial mode solver described above has been adapted for uniaxially anisotropic materials. For uniaxial anisotropic materials, the diagonal elements of the permittivity tensor are non-zero and not all equal.

For uniaxially anisotropic media, equations (2.17) and (2.18) are modified as follows,

$$\frac{\partial^2}{\partial y^2}E_x + \frac{\partial}{\partial x}\left(\frac{1}{\epsilon_{xx}}\left(\frac{\partial}{\partial x}(\epsilon_{xx}E_x) + \frac{\partial}{\partial y}(\epsilon_{yy}E_y)\right)\right) - \frac{\partial^2}{\partial x \partial y}E_y + (\omega^2\mu\epsilon_{xx} - \beta^2)E_x = 0 \tag{2.26}$$

$$\frac{\partial^2}{\partial x^2}E_y + \frac{\partial}{\partial y}\left(\frac{1}{\epsilon_{yy}}\left(\frac{\partial}{\partial x}(\epsilon_{xx}E_x) + \frac{\partial}{\partial y}(\epsilon_{yy}E_y)\right)\right) - \frac{\partial^2}{\partial x \partial y}E_x + (\omega^2\mu\epsilon_{yy} - \beta^2)E_y = 0 \tag{2.27}$$

The rest of the derivation remains same as the full-vectorial mode solver described in previous section.

2.3.4 Full-Vectorial Mode Solver For Bent waveguides

For bent waveguides equation (2.6) is no longer valid. Therefore, assuming following conditions,

$$\begin{aligned} \frac{\partial \epsilon}{\partial \phi} &= 0 \\ \frac{\partial}{r^2 \partial \phi^2}\vec{E} &= -\beta^2 \vec{E} \end{aligned}$$

To arrive at the eigenmode equations for bent waveguides, the wave equations are written in cylindrical coordinates. we start with equation (2.14) in cylindrical coordinates.

$$\begin{aligned}
\nabla^2\vec{E} + \nabla(\vec{E}.\frac{\nabla\epsilon}{\epsilon}) + (\omega^2\mu\epsilon)\vec{E} &= 0 \\
\frac{1}{r}\frac{\partial}{\partial r}(r\frac{\partial}{\partial r}E_r) + \frac{1}{r^2}\frac{\partial^2}{\partial\phi}E_r + \frac{\partial^2}{\partial y^2}E_r + \frac{\partial}{\partial r}\left(\frac{E_r}{\epsilon}\frac{\partial\epsilon}{\partial r} + \frac{E_\phi}{\epsilon}\frac{\partial\epsilon}{r\partial\phi} + \frac{E_y}{\epsilon}\frac{\partial\epsilon}{\partial y}\right) + (\omega^2\mu\epsilon)E_r &= 0 \\
\frac{1}{r}\frac{\partial}{\partial r}(r\frac{\partial}{\partial r}E_y) + \frac{1}{r^2}\frac{\partial^2}{\partial\phi}E_y + \frac{\partial^2}{\partial y^2}E_y + \frac{\partial}{\partial y}\left(\frac{E_r}{\epsilon}\frac{\partial\epsilon}{\partial r} + \frac{E_\phi}{\epsilon}\frac{\partial\epsilon}{r\partial\phi} + \frac{E_y}{\epsilon}\frac{\partial\epsilon}{\partial y}\right) + (\omega^2\mu\epsilon)E_y &= 0
\end{aligned}$$

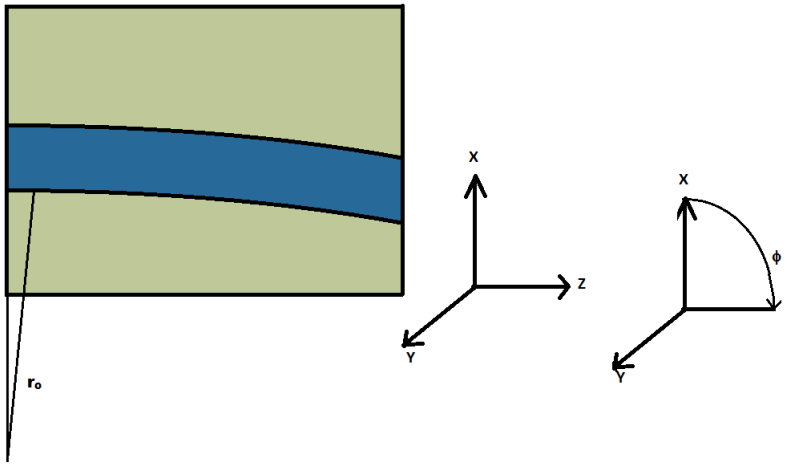

Figure 2.4: Axes for bent waveguides (Top view).
The blue region is the core of the waveguide. Gray region is the slab/cladding of the waveguide. r_0= radius of curvature of the bend.

To use the above equation, we use the following transformations.

$$\begin{aligned}
dx &= r\cos\phi \\
dy &= dy \\
dz &= r\sin\phi
\end{aligned}$$

for $\phi \approx 0$,

$$dz \approx r \times d\phi$$

This gives the following equations,

$$\begin{aligned}
\frac{1}{r}\frac{\partial}{\partial r}(r\frac{\partial}{\partial r}E_r) + \frac{\partial^2}{\partial y^2}E_r + \frac{\partial}{\partial r}\left(\frac{E_r}{\epsilon}\frac{\partial \epsilon}{\partial r} + \frac{E_y}{\epsilon}\frac{\partial \epsilon}{\partial y}\right) + (\omega^2\mu\epsilon - \beta^2)E_r &= 0 \\
\frac{1}{r}\frac{\partial}{\partial r}(r\frac{\partial}{\partial r}E_y) + \frac{\partial^2}{\partial y^2}E_y + \frac{\partial}{\partial y}\left(\frac{E_r}{\epsilon}\frac{\partial \epsilon}{\partial r} + \frac{E_y}{\epsilon}\frac{\partial \epsilon}{\partial y}\right) + (\omega^2\mu\epsilon - \beta^2)E_y &= 0
\end{aligned}$$

Thus we get two wave equations with only E_r and E_y components. These two equations can be solved using the method in section **1.2.1.**

To get E_x component of the waveguide, we use, when $\phi \approx 0$, $E_x = E_r$.

2.4 Simulations and Results

In the figure 1.6 , $r = h/H$ and $a/b = w/H$, where w = rib width, h = slab height. The single mode condition obtained the Full Vectorial mode solver described in this thesis has been compared with the single mode conditions obtained by Soref's curve (1) and Effective Index method (EIM).

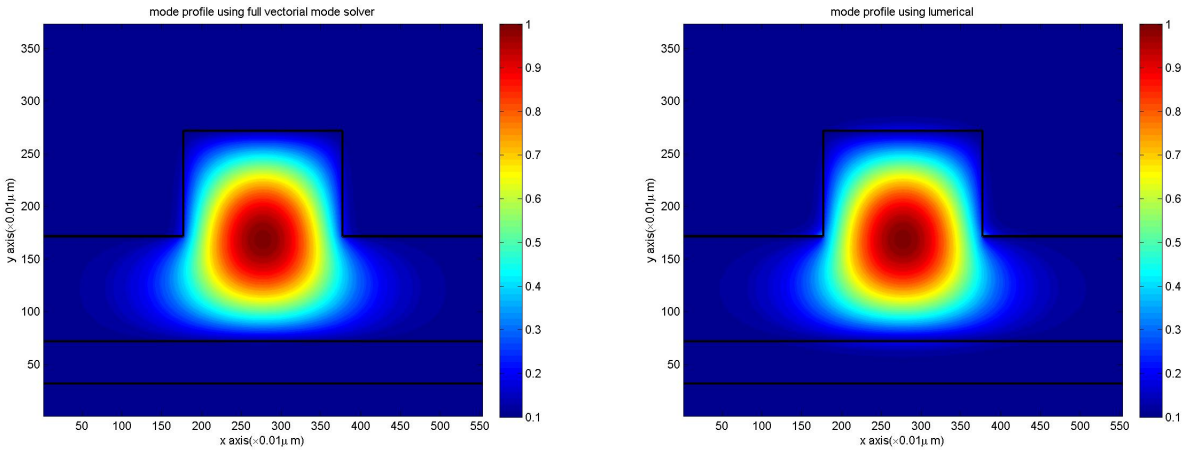

Figure 2.5: comparison of mode profiles of fundamental TE mode calculated using lumerical's mode solver, and full-vectorial mode solver described in this thesis.
Waveguide(n_{core}=3.477) dimensions: Rib Height=2μm, Rib Width=2μm,Slab height=1μm with SiO_2(n_{SiO_2}=1.45) below and Air (n_{Air}=1) above the waveguide.

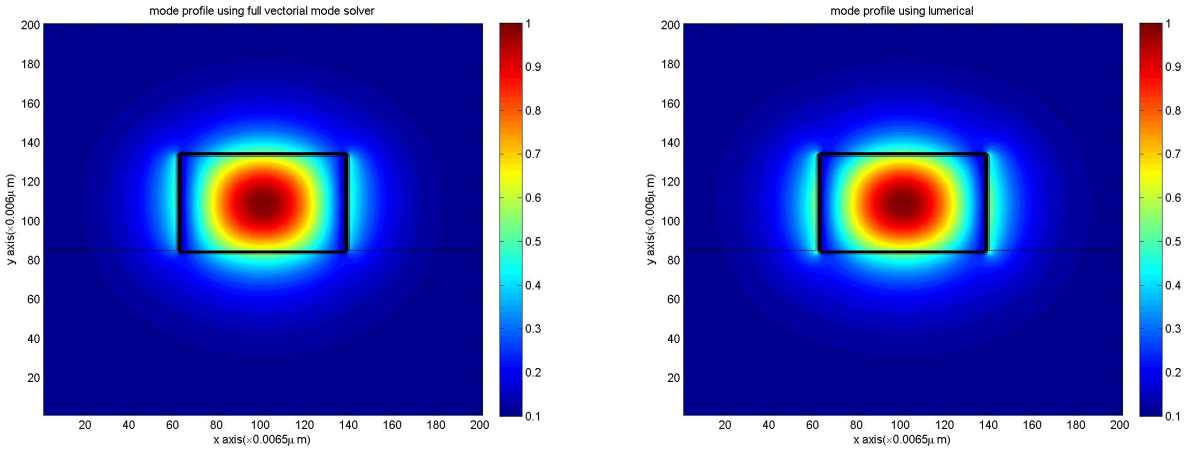

Figure 2.6: Mode profile of TE mode for photonic wire waveguide
Waveguide(n_{core}=3.477) dimensions = ($500nm \times 300nm$) with SiO_2(n_{SiO_2}=1.45) below and Air (n_{Air}=1) above.

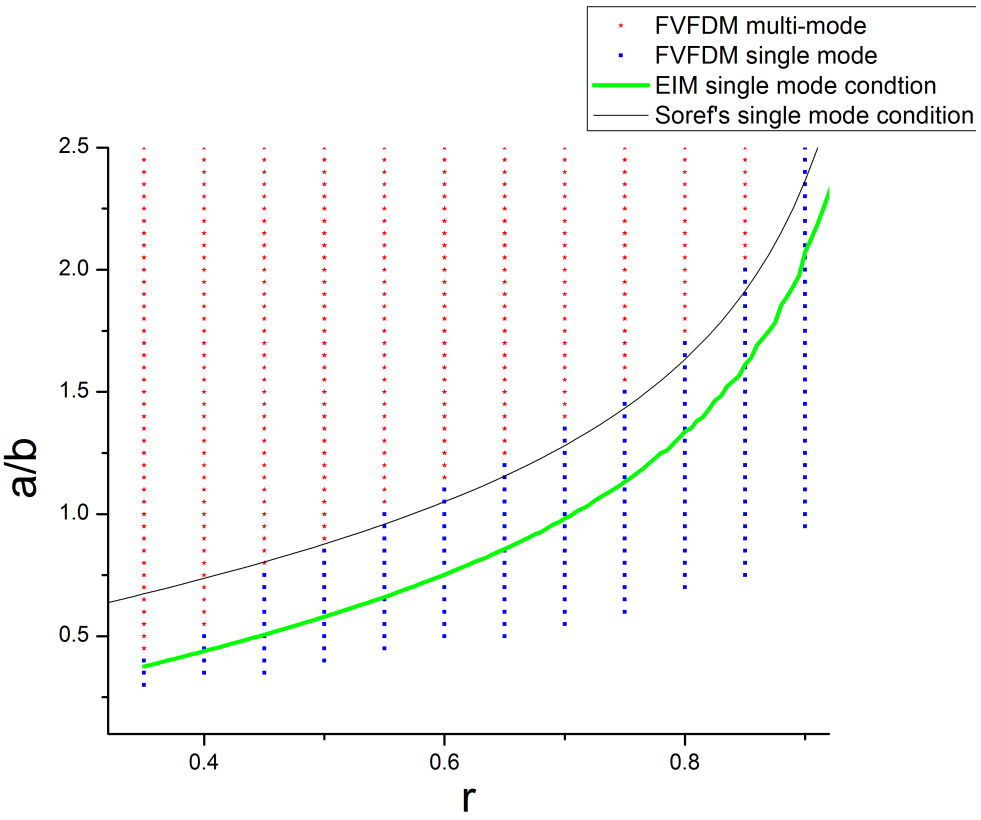

Figure 2.7: Analysis of single-mode condition for SOI rib waveguide structures with rib height = $10\mu m$

Table 2.1: Comparison of effective indices for DC using symmetric and antisymmetric boundary conditions with simulation of full structure

n_{eff} using full vectorial for Directional coupler	n_{eff} using symmetric boundary condition	n_{eff} us
3.3681	3.3681	
3.3673	-	
3.3592	3.3591	
3.3590	-	
3.2625	3.2625	
3.2164	-	
3.2076	3.2078	
3.2005	-	

In the figure, Rib height=$1\mu m$, Rib width = $1\mu m$, slab height = $0.5\mu m$, Separation between waveguides= $1\mu m$.

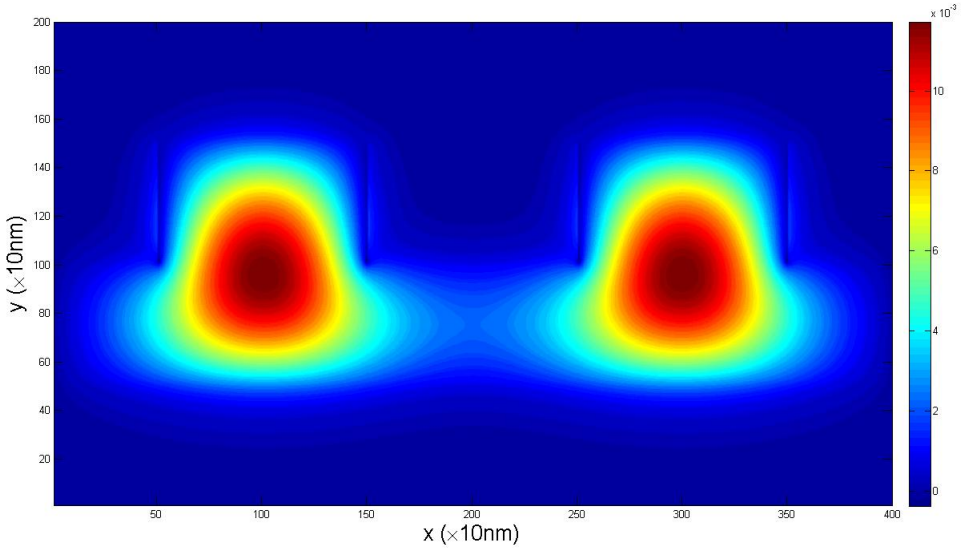

Figure 2.8: Directional coupler symmetric TE mode (Ex field)
In the figure, Rib height=$1\mu m$, Rib width = $1\mu m$, slab height = $0.5\mu m$, Separation between waveguides= $1\mu m$.

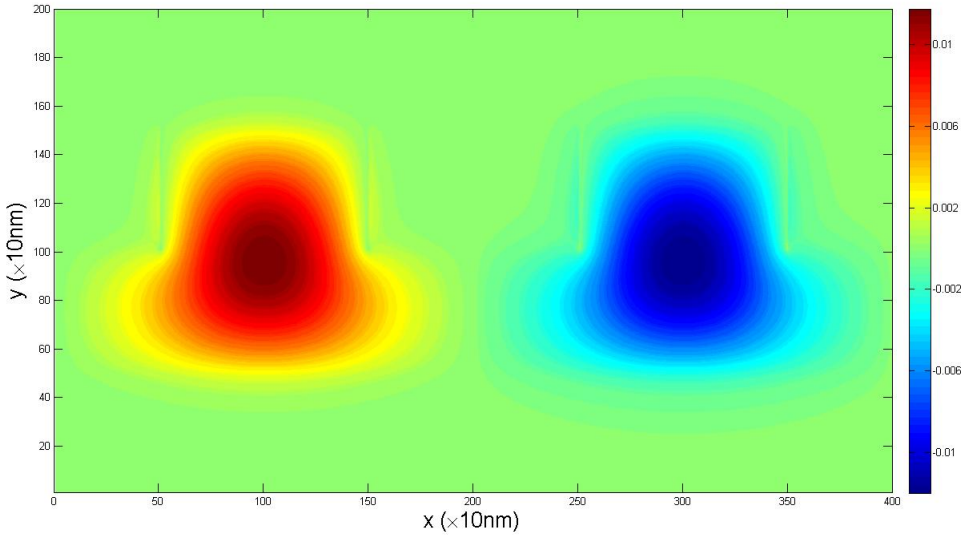

Figure 2.9: Directional coupler antisymmetric TE mode (Ex field)
In the figure, Rib height=$1\mu m$, Rib width = $1\mu m$, slab height = $0.5\mu m$, Separation between waveguides= $1\mu m$.

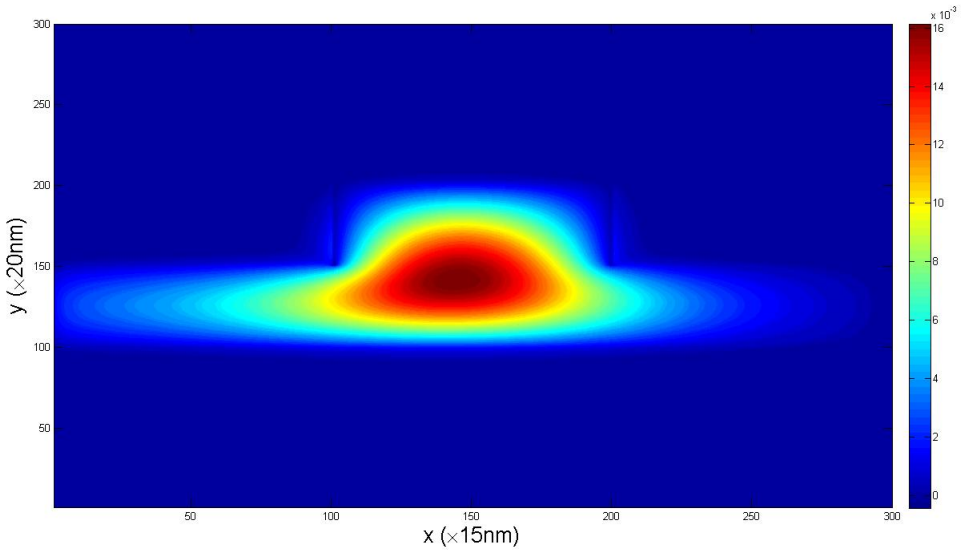

Figure 2.10: Field profile for TE mode for a bend waveguide
In this figure, Rib width = $1.5\mu m$, Rib height = $2\mu m$, slab height = $1\mu m$, Bend radius = $10\mu m$. The center of the bend circle is towards the right of the structure. As expected the field profile is shifted towards the left.

CHAPTER 3

Compound FDTD Method for Silicon Photonics

3.1 Introduction

Silicon exhibits third-order non-linear susceptibility $\chi^{(3)}$. The imaginary part of this susceptibility leads to Two Photon Absorption (TPA). TPA, in turn, leads to the generation of free carriers. These free carriers affect both real and imaginary part of the refractive index. This causes the waveguide to show Free Carrier Absorption (FCA) and free carrier plasma dispersion effects. Therefore TPA is an important effect as it creates free carriers along with its own nonlinear losses. Silicon also exhibits Raman effect and Kerr effects which can be modeled using the Drude-Lorentz model.

While the Kerr effect and Raman effect and free carrier plasma dispersion effect change the real part of the refractive index of the medium, we implement these effects through their respective polarization currents. Since FCA and TPA affect the absorption coefficient of the material, ie the imaginary part of the refractive index, these two effects can be included in the conductivity of the material. Since we are using frequency domain models for Kerr and Raman effects, we use Auxiliary Differential Equation method to find out their polarization currents in time domain.

3.2 FDTD Method

We start with Maxwell's Equations in time domain.

$$\nabla.\vec{D} = 0 \tag{3.1}$$

$$\nabla.\vec{H} = 0 \tag{3.2}$$

$$\nabla \times \vec{E} = -\mu_0 \frac{\partial \vec{H}}{\partial t} \tag{3.3}$$

$$\nabla \times \vec{H} = \frac{\partial(\vec{D})}{\partial t} + \sigma \vec{E} \tag{3.4}$$

Equations (3.1) and (3.2) represent static charges, and therefore are not involved in FDTD method for optical waveguides. Equations (3.3) and (3.4) are solved using leapfrog method(4).

This involves solving equations (3.3) and (3.4) at successive timesteps but not simultaneously.

In this thesis, Electric fields have been updated at timestep n and magnetic fields at $n + \frac{1}{2}$, where n is an integer.Spatially, the fields are staggered and the grid is shown in figure **??**.

In this thesis, FDTD method has been implemented for TM_Z mode. In TM_Z mode the only fields present are H_x, H_y, E_z.

Therefore,

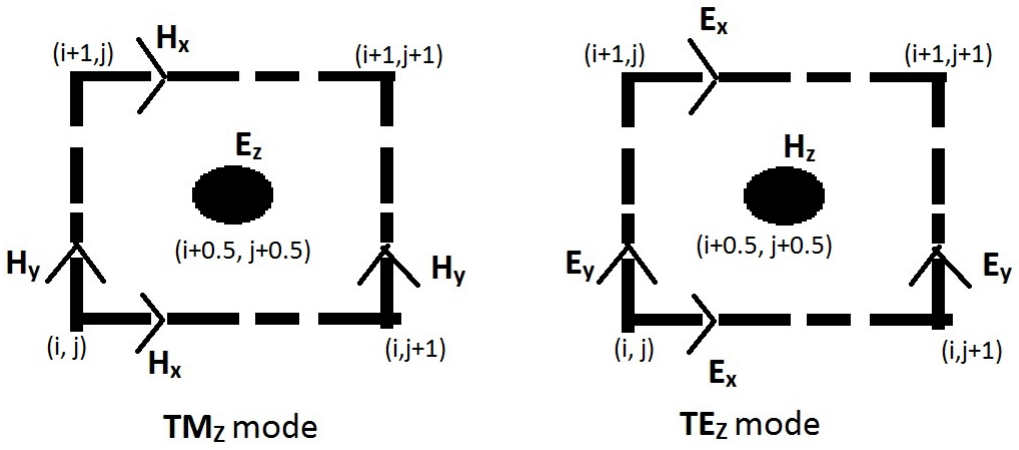

Figure 3.1: Yee's cell meshing for FDTD

For TM_z mode, H_x, H_y are defined at integral grid points while E_z is defined at half integral grid points.
For TE_z mode, E_x, E_y are defined at integral grid points while H_z is defined at half integral grid points.

$$\vec{H} = H_x\hat{a}_x + H_y\hat{a}_y$$
$$\vec{E} = E_z\hat{a}_z \tag{3.5}$$

For TE_Z , the field vectors are,

$$\vec{H} = H_z\hat{a}_z$$
$$\vec{E} = E_x\hat{a}_x + E_y\hat{a}_y \tag{3.6}$$

3.3 The Compound FDTD Method

3.3.1 Methodology

For the first half time step, $\vec{H}$ field is updated using equation (3.3)

$$\nabla \times \vec{E} = -\mu_0 \frac{\partial \vec{H}}{\partial t}$$

For the second half time step, $\vec{E}$ field is updated using the following scheme(3).

Starting with equation (3.4),

$$\begin{aligned} \nabla \times \vec{H} &= \frac{\partial(\vec{D})}{\partial t} + \sigma \vec{E} \\ \nabla \times \vec{H} &= \epsilon_0 \epsilon_r \frac{\partial}{\partial t} \vec{E} + \sigma \vec{E} + \vec{J}_L + \vec{J}_{NL} \end{aligned} \tag{3.7}$$

Here,

$$\begin{aligned} \vec{D} &= \epsilon_0 \epsilon_r \vec{E} + \vec{P}_L + \vec{P}_{NL} \\ \vec{P}_{NL} &= \vec{P}_R + \vec{P}_K + \vec{P}_P \\ \vec{J}_L &= \frac{\partial}{\partial t} \vec{P}_L \\ \vec{J}_{NL} &= \frac{\partial}{\partial t} \vec{P}_{NL} \\ \sigma &= \sigma_0 + \sigma_{TPA} + \sigma_{FCA} \end{aligned}$$

where,

$\vec{P}_L$=> Linear Polarization

$\vec{P}_N L$=> Nonlinear Polarization

$\vec{P}_R$=> Polarization due to Raman Effect

$\vec{P}_K$=> Polarization due to Kerr Effect

$\vec{P}_P$=> Polarization due to Plasma dispersion effect

σ_0=> inherent conductivity

σ_{TPA}=> conductivity due to Two Photon Absorption

σ_{FCA}=> conductivity due to Free Carrier Absorption

3.3.2 Linear Polarization

For linear polarization,

$$\vec{P}_L = \chi_L \vec{E}$$
$$\vec{J}_L = \jmath\omega\chi_L \vec{E}$$

where the susceptibility χ_L is given in the frequency domain by the Drude-Lorentz model,

$$\chi_L = \frac{\Delta\epsilon_L \omega_L^2}{\omega_L^2 + \jmath\gamma_L\omega - \omega^2}$$

Therefore, in frequency domain, $\vec{J}_L$ is given by

$$\vec{J_L} = \frac{\jmath\omega\Delta\epsilon_L\omega_L^2}{\omega_L^2 + \jmath\omega_L\omega - \omega^2}\vec{E}$$

This gives rise to the time domain equation around time step n,

$$\vec{J}_L^{n+\frac{1}{2}} = \frac{(\alpha_{2L}+1)}{2}\vec{J}_L^n + \frac{\alpha_{1L}}{2}\vec{J}_L^{n-1} + \frac{\alpha_{3L}}{2}(\vec{E}^{n+1} - \vec{E}^{n-1}) \tag{3.8}$$

where,

$$\begin{aligned}
\alpha_{1L} &= \frac{\gamma_L\Delta t - 2}{\gamma_L\Delta t + 2} \\
\alpha_{2L} &= \frac{4 - 2(\Delta t\omega_L)^2}{\gamma_L\Delta t + 2} \\
\alpha_{3L} &= \frac{\epsilon_0\Delta\epsilon_L\omega_L^2\Delta t}{\gamma_L\Delta t + 2}
\end{aligned}$$

3.3.3 Raman Effect

Raman susceptibility is also modified using nonlinear Lorentz model(6)

$$\chi_R = \frac{\Delta\epsilon_R\omega_R^2 \left|E_z\right|^2}{\omega_R^2 + \jmath\gamma_R\omega - \omega^2}$$

Polarization current due to Raman Effect is given by,

$$\vec{J_R} = \frac{\jmath\omega\Delta\epsilon_R\omega_R^2 \left|\vec{E}\right|^2}{\omega_R^2 + \jmath\gamma_R\omega - \omega^2}\vec{E}$$

When transforming into time domain, we encounter the term $\jmath\omega \left|\vec{E}\right|^2 \vec{E}$.

For TM_Z mode, in time domain,

$$\frac{\partial}{\partial t}(\left|\vec{E}\right|^2 \vec{E}) = 3(E_z)^2 \frac{\partial}{\partial t} E_z \tag{3.9}$$

while for TE_Z mode, in time domain,

$$\begin{aligned}
\frac{\partial}{\partial t}(\left|\vec{E}\right|^2 \vec{E}) &= \frac{\partial}{\partial t}((E_x^2 + E_y^2)(E_x \hat{a_x} + E_y \hat{a_y})) \\
\frac{\partial}{\partial t}(\left|\vec{E}\right|^2 E_x) &= (E_y^2 + 3E_x^2)\frac{\partial}{\partial t} E_x + 2E_x E_y \frac{\partial}{\partial t} E_y \\
\frac{\partial}{\partial t}(\left|\vec{E}\right|^2 E_y) &= (E_x^2 + 3E_y^2)\frac{\partial}{\partial t} E_y + 2E_x E_y \frac{\partial}{\partial t} E_x
\end{aligned}$$

Thus Polarization current due to Raman Effect is given for TM_Z mode, in time domain, by

$$J_L^{n+\frac{1}{2}} = \frac{(\alpha_{2L} + 1)}{2} \vec{J}_L^n + \frac{\alpha_{1L}}{2} J_L^{n-1} + \frac{\alpha_{3L}}{2}(E_z^{n+1} - E_z^{n-1}) \tag{3.10}$$

where,

$$\begin{aligned}
\alpha_{1R} &= \frac{\gamma_R \Delta t - 2}{\gamma_R \Delta t + 2} \\
\alpha_{2R} &= \frac{4 - 2(\Delta t \omega_R)^2}{\gamma_L \Delta t + 2} \\
\alpha_{3R} &= \frac{\epsilon_0 \Delta \epsilon_R \omega_R^2 \Delta t}{\gamma_R \Delta t + 2} \times 3 \left|E_z\right|^2
\end{aligned}$$

3.3.4 Kerr Effect

For Kerr Effect, susceptibility is given by non-linear Debye model(7),

$$\chi_K = \frac{\epsilon_2 \left|E_z\right|^2}{1 + \jmath\omega\tau_k}$$

Therefore in time domain, we get

$$J_K^{n+\frac{1}{2}} = \alpha_{1K} J_K^{n-\frac{1}{2}} + \alpha_{2K}(E_z^{n+1} - E_z^{n-1}) \tag{3.11}$$

where,

$$\alpha_{1K} = \frac{2\tau_K - \Delta t}{2\tau_K + \Delta t}$$
$$\alpha_{2K} = \frac{\epsilon_0\epsilon_2}{2\tau_K + \Delta t} \times 3\left|E_z\right|^2$$

3.3.5 Two Photon Absorption

Implementing TPA related absorption into conductivity(8) we update only the conductivity in the FDTD update equation (3.7).

$$\sigma_{TPA} = \alpha_{TPA} n c \epsilon_0$$

TPA Absorption is given by

$$\alpha_{TPA} = \beta_{TPA} I = \frac{cn\epsilon_0 \beta_{TPA}}{2} |E_z|^2$$
$$\sigma_{TPA} = \frac{c^2 n^2 \epsilon_0^2 \beta_{TPA}}{2} |E_z|^2 \tag{3.12}$$

3.3.6 Free Carrier Absorption

Carrier conductivity equivalent to Free Carrier Absorption (FCA) is given by,

$$\sigma_{FCA} = \alpha_{FCA} nc\epsilon_0 \tag{3.13}$$

The absorption coefficient is given by(9),

$$\alpha_{FCA} = \bar{\sigma}_{FCA,e} N_e + \bar{\sigma}_{FCA,h} N_h$$

where $\bar{\sigma}_{FCA,e}$ and $\bar{\sigma}_{FCA,h}$ are FCA cross sections of electrons and holes respectively and are given by(10),

$$\bar{\sigma}_{FCA,e} = 8.85 \times 10^{-18} \big(\frac{\lambda[\mu m]}{1.55}\big)^2$$
$$\bar{\sigma}_{FCA,h} = 6.0 \times 10^{-18} \big(\frac{\lambda[\mu m]}{1.55}\big)^2$$

Assuming Drift , Diffusion and other generation/recombination effects are negligible, we use the following rate equation,

$$\frac{\partial N}{\partial t} = \frac{1}{2\hbar\omega}(\beta_{TPA} I^2) - \frac{N}{\tau_r}$$

This gives rise to the update equation for carrier concentration,

$$N^{n+\frac{1}{2}} = \frac{2\tau_r - \Delta t}{2\tau_r + \Delta t} N^{n-\frac{1}{2}} + \frac{\tau_r \Delta t}{2\tau_r + \Delta t} \frac{c^2 n^2 \epsilon_0^2 \beta_{TPA}}{4\hbar\omega} |E_z^n|^4 \tag{3.14}$$

3.3.7 Plasma Dispersion

Using equation (3.14) with the Soref's experimental fit(9) we get update equation for current due to plasma dispersion effect.

$$\Delta n_{plasma} = (-8.8 \times 10^{-22} N_e - 8.5 \times 10^{-18} N_h^{0.8}) \big(\frac{\lambda[\mu m]}{1.55}\big)^2 \tag{3.15}$$

$$J_P^{n+\frac{1}{2}} = 2\epsilon_0 n \big(\Delta n_{plasma}(E_z^{n+1}) E_Z^{n+1} - \Delta n_{plasma}(E_z^n) E_Z^n\big) \tag{3.16}$$

3.3.8 The combined equation

Using equations (3.7) with equations (3.8), (3.10), (3.11), (3.12), (3.13), (3.16), gives the overall update equation,

$$\begin{aligned} A_1 E_z^{n+1} = A_2 E_z^n + A_3 E_z^{n-1} - \frac{\alpha_{1L}}{2} J_L^{n-1} - \frac{1+\alpha_{2L}}{2} J_L^n \\ - \frac{\alpha_{1L}}{2} J_R^{n-1} - \frac{1+\alpha_{2L}}{2} J_R^n - \alpha_{1K} J_K^{n-\frac{1}{2}} \\ + (\nabla \times H)_z^{n+\frac{1}{2}} - J_P^{n+\frac{1}{2}} \end{aligned} \tag{3.17}$$

where,

$$A_1 = \frac{\epsilon_0 \epsilon_r}{\Delta t} + \frac{\alpha_{3L}}{2} + \frac{\alpha_{3R}}{2} + \alpha_{2K} + \frac{\sigma^{n+\frac{1}{2}}}{2}$$
$$A_2 = \frac{\alpha_{3L}}{2} + \frac{\alpha_{3R}}{2} + \alpha_{2K}$$
$$A_3 = \frac{\epsilon_0 \epsilon_r}{\Delta t} - \frac{\sigma^{n+\frac{1}{2}}}{2}$$

3.4 Simulations and Results

3.4.1 Simulation method

The simulation is done in 2D FDTD. In 2D, there are two modes present. Here, only the TM_Z mode has been presented. For each time step, the H_x, H_y fields are updated first using equation (3.3). Then E_z field is updated using equation (3.17). Since, the coefficients α_{3R} and α_{2K} depend on $|E_z|^2$ these are updated at every time step. The carrier concentration N and the conductivities are also updated at every time step. Since update equation (3.16) for J_P requires electric field at the same time step, equation (3.17) is updated without using J_P first. Then, the total electric field and J_P are found by using equation (3.16) in an iterative loop. It has been found that only 3-4 iteration loops are required in general. Therefore, the iterations do not add much to the computation costs.

Refractive index change due to Kerr effect is given by,

$$\Delta n_{kerr} = n_2^{'} I$$

This change is added to the refractive index profile of the simulated structure before entering the iteration loop for including plasma dispersion effect.

Refractive index change due to Plasma Dispersion effect is given by equation (3.15).

The conductivity used in update equation (3.17) is given by,

$$\sigma = \sigma_0 + \sigma_{TPA} + \sigma_{FCA}$$

Here, σ_0 is conductivity due to inherent losses, which is assumed to be negligible for Silicon waveguides.

3.4.2 Simulation Setup And Parameters

The compound FDTD method is used to simulate an SOI waveguide of dimensions $(450nm \times 200nm)$. The simulation is done for 2D FDTD using the method used in (some reference). Here, the core index is taken as n=3.043, while the SiO_2 index is taken as n=1.45. The rest of the parameters used in the simulation are given in Table 2.1.

The simulation region is terminated using Gedney's CPML(4).

The material parameters used in the simulations are the same as in (3).

Table 3.1: Parameter values used in the simulations in CFDTD

Parameter	Value	Units
λ	1.49	μm
E_{max}	6.1971×10^8	V/m
$FWHM$	200	fs
n_{SiO_2}	1.5	-
n_{air}	1.0	–
n_{Si}	3.043	–
Δx	20	nm
Δy	20	nm
Δt	23.57	as
l_x	100	μm
l_y	1.6	μm
$n_2^,$	7×10^{-18}	m^2/W
β_{TPA}	9×10^{-3}	m/GW
τ_{kerr}	0	s
τ_r	0.8	ns
ω_R	15.6	THz
γ_R	106	GHz
ϵ_R	76.10×10^{-21}	m^2/V^2

3.4.3 Results

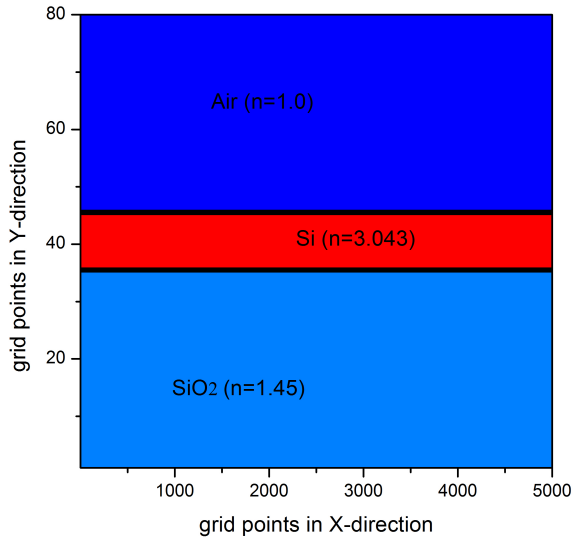

Figure 3.2: Refractive index profile used in the simulation

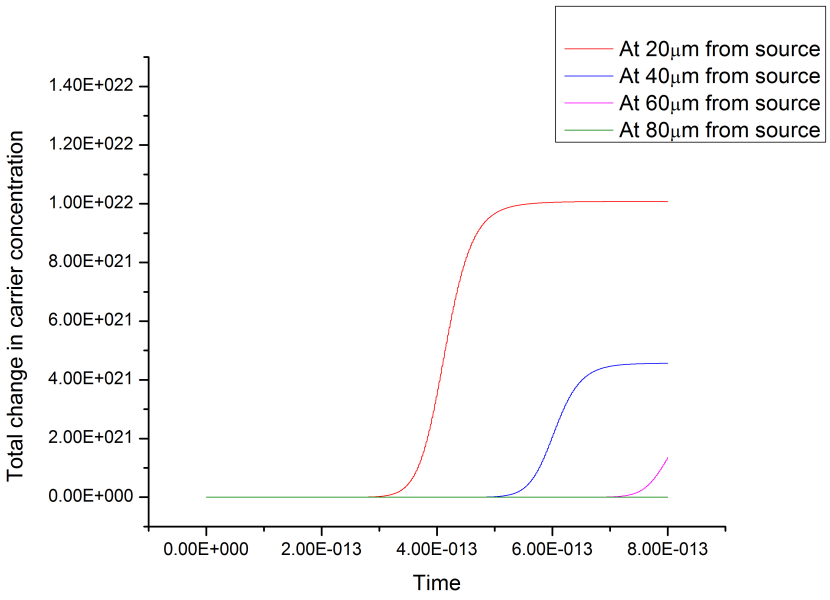

Figure 3.3: Change in carrier concentration

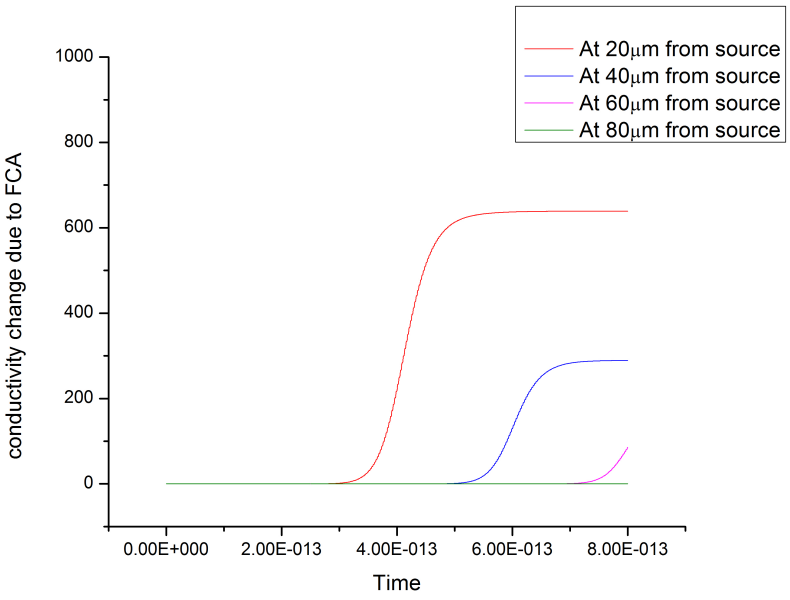

Figure 3.4: Conductivity change due to FCA

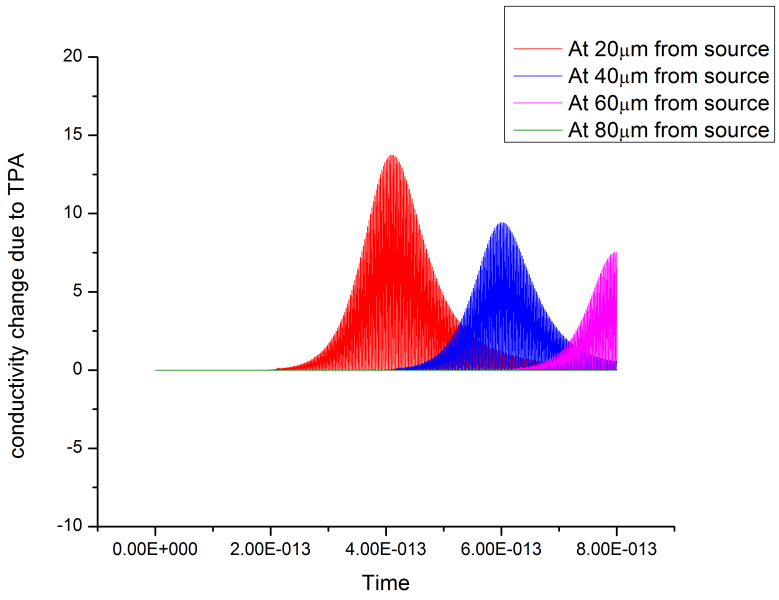

Figure 3.5: Conductivity change due to TPA

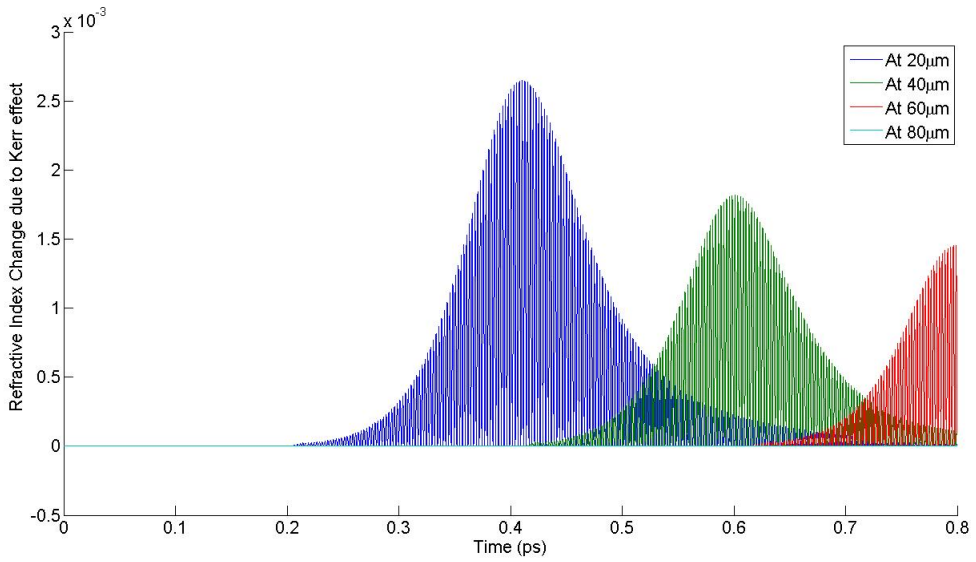

Figure 3.6: Refractive index change due Kerr effect

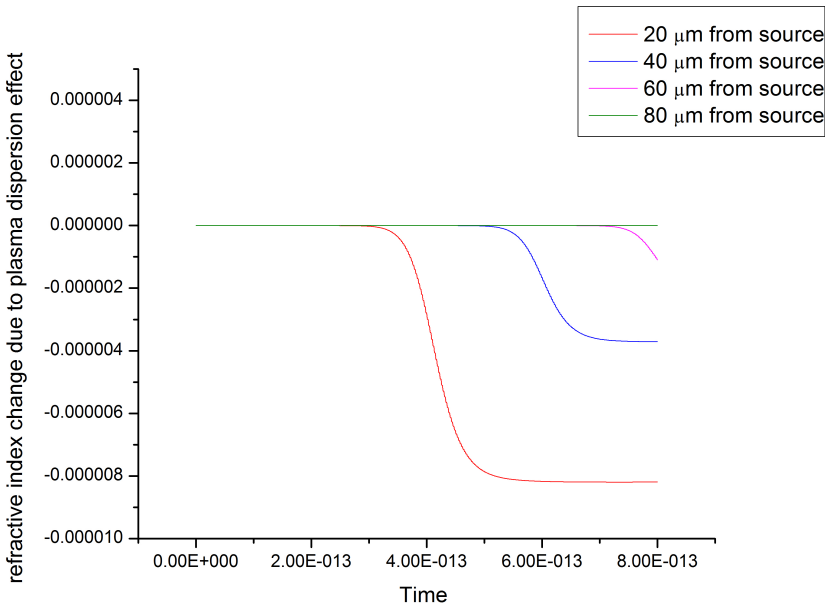

Figure 3.7: Refractive index change due to plasma dispersion effect

CHAPTER 4

Conclusions

4.1 Summary

Semi-vectorial, Full-Vectorial mode solvers have been developed for straight and bent waveguides with isotropic materials. The mode solvers have also been adopted for uniaxially anisotropic waveguides.

In the second part, An FDTD method for 3rd order non-linear materials has been given and the results have been shown. This method has also been implemented using OpenCL on GPU. The running times have not been compared but it has been observed that OpenCL code gives faster results.

4.2 Future Works

The mode solvers have been implemented for uniaxially anisotropic materials. Therefore, the UPML can be implemented to see and try if the mode solver can be improved. Other methods of finding modes can be compared with this mode solver to compare and improve the performances.

Due to straightforward formulation of finite difference equations, various interfaces and boundary conditions can be analyzed and inserted in the eigenvalue equations. Further analysis of the numerical error in the mode solver can help in improving the performance of the mode solver.

The compound FDTD method is currently implemented for third order non-linearity. In the future, second order non-linearity can be implemented and the FDTD method can be appropriately adjusted for non-linear materials like $LiNbO_3$.

The FDTD method can be accelerated using GPU languages like CUDA and OpenCL. When the sparse linear algebra libraries get developed for these languages, it will be possible to implement the mode solver in GPU.

REFERENCES

[1] Arman B. Fallahkhair, Kai S. Li, and Thomas E. Murphy, "Vector Finite Difference Modesolver for Anisotropic Dielectric Waveguides",Journal Of Lightwave Technology, Vol. 26, No. 11, 2008.

[2] R. A. Soref, J. Schmidtchen, and K. Petermann, "Large single mode RIB waveguides in GeSi-Si and Si-on-SiO 2 ," IEEE J. Quantum Electron., vol. 27, pp. 1971–1974, 1991.

[3] Abbas Olyaee and Farzad T. Hamadani, "Compound FDTD method for silicon photonics", AIP Advances 1, 032107 (2011).

[4] Stephen D. Gedney, and Bo Zhao,"An Auxiliary Differential Equation Formulation for the Complex-Frequency Shifted PML",IEEE Transactions On Antennas And Propagation, Vol. 58, No. 3, March 2010.

[5] Allen Taflove, Susan Hagness, "Computational Electrodynamics: The Finite-Difference Time-Domain Method", Artech House.

[6] R. W. Boyd, "Non-linear Optics", Academic Press.

[7] R. W. Ziolkowski, J. B. Judkins, "Full-wave Vector Maxwell equation modelling of the self-focusing of ultrashort optical pulses in a nonlinear Kerr medium exhibiting a finite response time". Optics J Soc Amr **10**, 1993.

[8] I. S. Maksymov, L. F. Marshall, J. Pallares, " Modelling of two-photon absorption in nonlinear photonics crystal all-optical switch", Sci Dir Opt Communications **269**, 2007.

[9] R. Soref, B. R. Bennett, “Electrooptical Effects in Silicon”, IEEE J Quantum Electron **23,** 1987.

[10] R. Soref, B. R. Bennet, “Kramers-Kronig analysis of electrooptical switching in silicon”, Proc SPIE **704**, 1987.